Earth's Future

RESEARCH ARTICLE
10.1029/2025EF007875

Storm Surge Barriers Reduce Seaward Sediment Supply to Lagoonal Estuaries

David K. Ralston[1], Philip M. Orton[2], John C. Warner[3], and Shima Kasaei[2]

[1]Applied Ocean Physics & Engineering, Woods Hole Oceanographic Institution, Woods Hole, MA, USA, [2]Civil, Environmental & Ocean Engineering, Stevens Institute of Technology, Hoboken, NJ, USA, [3]United States Geologic Survey, Woods Hole Coastal & Marine Science Center, Woods Hole, MA, USA

Key Points:

- Storm surge barrier infrastructure constricts tidal flow, increasing drag and reducing tidal amplitude in a lagoonal estuary
- Sediment import from the coastal zone due to tidal asymmetry is reduced, more so for fine sand (20%) than silt (3%) or fine silt (<1%)
- Reductions in sediment supply could adversely impact salt marshes, both natural and restored, which also protect against storm surge

Correspondence to:
D. K. Ralston,
dralston@whoi.edu

Citation:
Ralston, D. K., Orton, P. M., Warner, J. C., & Kasaei, S. (2026). Storm surge barriers reduce seaward sediment supply to lagoonal estuaries. *Earth's Future*, *14*, e2025EF007875. https://doi.org/10.1029/2025EF007875

Received 1 DEC 2025
Accepted 14 APR 2026

Abstract Numerical simulations with realistic forcing of fixed infrastructure for a proposed storm surge barrier for a lagoonal estuary, Jamaica Bay (New York, USA), are analyzed during typical forcing conditions to assess alterations to flow and sediment transport with the barrier open. Lagoonal estuaries are shallow and have modest watershed freshwater and sediment inputs, so sediment delivery is primarily from offshore by tidal transport. The storm surge barrier infrastructure across the inlet channel reduces cross-sectional area and increases tidal velocities, increasing frictional and form drag. The overall reduction in tidal amplitude is about 1%, but the quarterdiurnal M_4 component decreases by 11%. The salinity and stratification in the estuary are only slightly modified by mixing by stronger velocities near the barrier. Sediment transport in the inlet scales approximately with tidal velocity cubed and net landward transport is driven by flood-dominant tidal asymmetry. Additionally, tidal asymmetry in the jet flow through barrier openings causes a divergence in sediment transport within several kilometers. The alterations to the tidal currents reduce sediment import to the bay by 20% for fine sand; transport of sediment with slower settling velocities is less affected, with reductions of 3% for medium silt and <1% for fine silt. The study examined tidal exchange with an open barrier, but the overall impact also depends on barrier operations during major storm events. The impacts of barrier infrastructure on lagoonal estuaries are distinct from other estuary types due to their modest freshwater input, predominance of tidal transport, and offshore sediment supply.

Plain Language Summary Storm surge barriers are one of the approaches being considered to protect coastal cities from damage by inundation with storm events. During typical conditions, barriers remain open to tidal flow but fixed infrastructure partially obstructs the flow compared to conditions without the barrier. A numerical model is used to assess potential impacts of a proposed barrier on tidal currents and sediment transport in Jamaica Bay (New York, USA). Jamaica Bay, like many similar lagoonal estuaries, is shallow, has little watershed input of runoff or sediment, and derives most of its sediment supply from the coastal ocean. Storm surge barrier infrastructure reduces the cross-sectional area of the inlet connecting to the ocean and thereby increases tidal velocities. Stronger currents cause more frictional energy loss from the tide, most notably in the tidal constituent that promotes landward sediment transport. The reductions in tidal energy with the barrier cause delivery of fine sand to the bay to decrease by 20%, with smaller changes in transport of finer, silt-sized sediment. The alterations to sediment delivery may reduce resilience of natural and restored salt marsh areas to sea level rise, which also affects coastal storm protection.

1. Introduction

Coastal cities around the world are increasingly threatened by inundation from storm events due to sea level rise, increased storm intensity, and expansion of urbanized areas. Various risk mitigation measures have been proposed to reduce flood impacts, including ecosystem-based measures and coastal defense infrastructure (Orton et al., 2023; Temmerman et al., 2013). Storm surge barriers use fixed and moveable infrastructure to isolate coastal regions during infrequent storm events but also allow for tidal exchange and navigation during non-storm periods (Rasmussen et al., 2020). Fixed infrastructure houses the gates during non-storm periods, reducing the cross-sectional flow area (Mooyaart & Jonkman, 2017). Barriers may also include dam sections that block flow entirely and further reduce the flow area. Storm surge barriers are increasingly prevalent, with examples including the Eastern Scheldt (Netherlands), Thames River (United Kingdom), St. Petersburg (Russia), and Venice Lagoon (Italy) (Mooyaart & Jonkman, 2017).

Since surge barriers and their associated infrastructure alter flow and transport during both storm events and non-storm conditions, it is critical to assess potential impacts. For example, surge barriers may negatively impact ecosystem-based mitigation measures like the creation of tidal wetlands, thereby affecting the overall inundation risk (Tognin et al., 2021). Extensive studies of changes to the Eastern Scheldt system since barrier construction in 1986 have identified changes in tidal amplitude, salinity, stratification, suspended sediment, morphology, and habitat conditions resulting from the alterations to flow by the barrier (Brand et al., 2016; de Vet et al., 2024). Structural alterations for the storm surge barrier for Venice Lagoon have also altered tidal propagation and sediment dynamics (Finotello et al., 2023; Matticchio et al., 2017; Scarpa et al., 2025). In deeper, partially mixed estuaries like Chesapeake Bay and the Hudson River, hydrodynamic models showed that flow restrictions from barrier infrastructure that decrease the tidal amplitude also increase the salinity intrusion and stratification. This study focuses on fixed infrastructure for surge barriers, but similar issues arise for any large, permanent coastal infrastructure that alter tidal exchange through an inlet such as bridge piers or sea walls.

Reductions in cross-sectional flow area by barrier infrastructure increase tidal velocities. The increased velocities through barrier openings cause increased drag and decreased tidal amplitude (Du et al., 2017; Nienhuis & Smaal, 1994; Ralston, 2022). The decrease in tidal amplitude can alter salinity dynamics inside the estuary, causing increased stratification and landward shifts in the salinity distribution (Brand et al., 2016; Ralston, 2022). In the Eastern Scheldt, reductions in sediment resuspension with reduced tidal amplitude led to changes in light availability and the phytoplankton community composition (Bakker et al., 1990).

Sediment transport can be altered both by the local increases in velocity at the barrier and by the overall decrease in tidal energy due to enhanced drag. Locally, increased tidal velocities enhance resuspension and bed scour near the barrier (Broekema et al., 2018). Inside the estuary, decreases in tidal amplitude and reduced tidal velocities can lead to infilling as tidal channels adjust to a new morphological equilibrium (de Vet et al., 2024; Eelkema et al., 2013). In the Eastern Scheldt, sediment accumulation in tidal channels came primarily from erosion of adjacent tidal flats by wind waves, resulting in deepening of the tidal flats (Brand et al., 2016), and sediment import from the North Sea was greatly reduced (Louters et al., 1998; Smaal & Nienhuis, 1992). Morphological adjustment continued for decades after barrier construction in 1986 as tidal channel shoaling and increased tidal prism with deepening of the flats approached a new equilibrium (de Vet et al., 2024). Alternatively, in estuaries where sediment supply comes predominantly from riverine sources, reductions in tidal amplitude and increased estuarine circulation can increase sediment retention and accumulation (Ralston, 2023). Changes in sediment availability and accumulation can have important implications for salt marsh resilience, as with reductions in sediment supply to marshes behind barriers for the Eastern Scheldt and Venice Lagoon (Louters et al., 1998; Tognin et al., 2022).

The focus of this study is on storm surge barriers being considered for New York City after Hurricane Sandy in 2012 caused loss of life and billions in property damages (Chen et al., 2020; Strauss et al., 2021). New York City is located on the Hudson-Raritan estuary and surrounding embayments, so surge barrier impacts depend on the location. Studies have examined a range of scenarios, including a barrier across the mouth of the Hudson that would be among the largest in the world as well as multiple smaller barriers (Kluijver et al., 2019; US Army Corps of Engineers, New York District, 2022). Numerical modeling of a proposed barrier at the mouth of the Hudson found that it would decrease tidal amplitude, increase stratification and the salinity intrusion, and increase sediment retention in the estuary (Chen & Orton, 2023; Ralston, 2022, 2023). In contrast, the focus of this study is on a proposed barrier for Jamaica Bay, a small lagoonal estuary with minimal freshwater and sediment inputs behind a barrier peninsula. The differences in forcing conditions affect the surge barrier impacts and are relevant to similar estuaries where freshwater inputs are small and sediment input comes primarily from offshore.

This study builds on previous model development for the Hudson-Raritan estuary but applies a high-resolution, nested-grid approach to simulate a realistic, open storm surge barrier during non-storm forcing conditions. Analysis of the model results examines changes in tidal range, velocity, and salinity conditions in Jamaica Bay, but the focus is on changes in sediment delivery to the estuary. Jamaica Bay has lost substantial salt marsh area due in part to limited sediment supply (Chant et al., 2021; Peteet et al., 2018), so modest changes to sediment availability could have substantial impacts on marsh sustainability. Jamaica Bay is representative of other coastal regions where sediment supply is limited and a major concern, and barriers are proposed for similar systems such as Barnegat Bay (NJ) and Galveston Bay (TX) (US Army Corps of Engineers, Galveston District & Texas General Land Office, 2021; US Army Corps of Engineers, Philadelphia District, 2021).

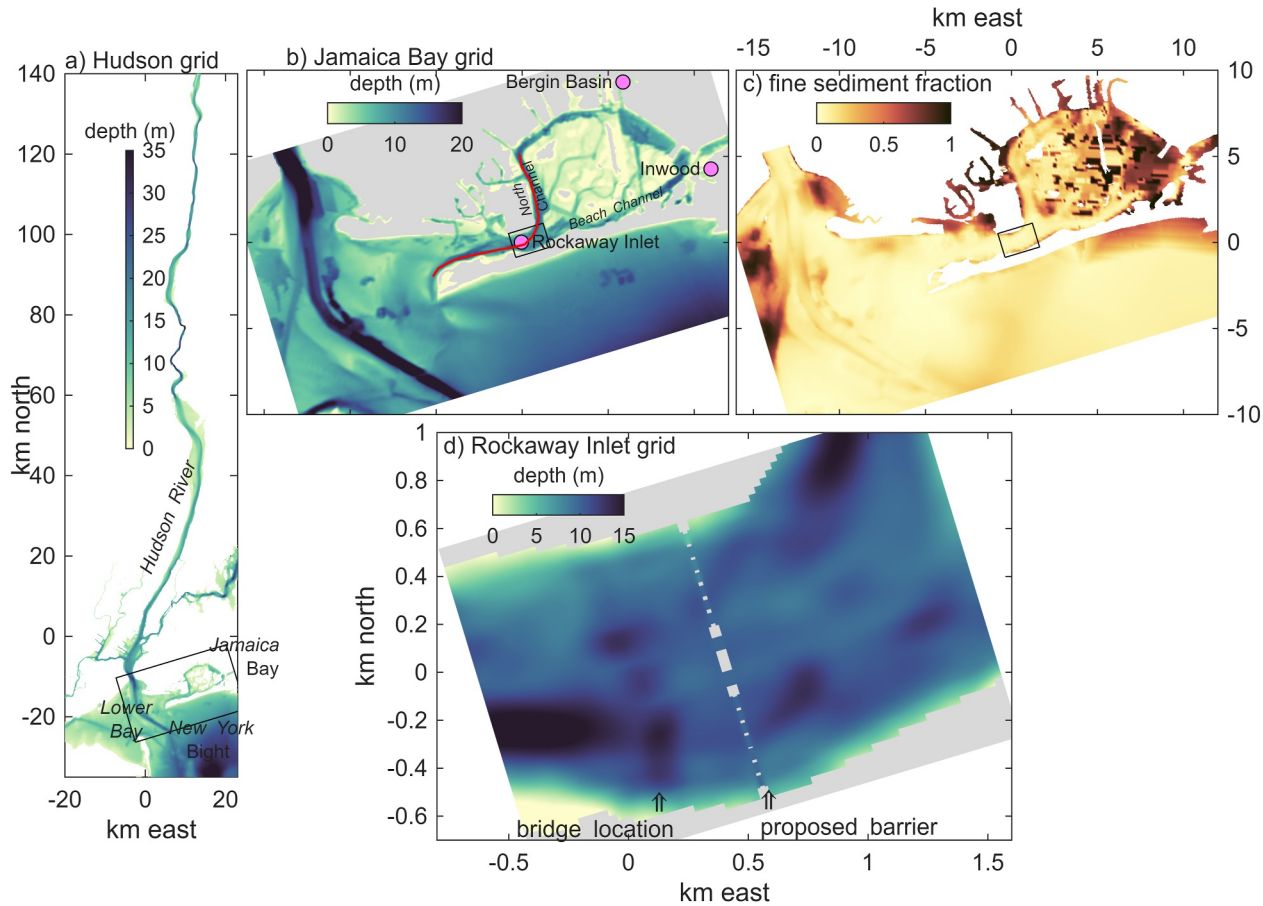

Figure 1. Model grid bathymetry. (a) Hudson River estuary model grid bathymetry, with black box outlining extent of Jamaica Bay grid. Note that the full Hudson grid extends north to the tidal limit at 225 km (not shown). (b) Jamaica Bay grid bathymetry, with black box outlining extent of Rockaway Inlet grid; red line shows transect in Figure 4. (c) Jamaica Bay initial bed sediment composition as fraction fine sediment (medium silt and fine silt size classes). (d) Rockaway Inlet grid with barrier infrastructure, noting location of Marine Parkway–Gil Hodges Bridge.

2. Methods

Jamaica Bay is a lagoonal estuary on the western end of Long Island, New York, USA. The bay is connected to New York Bight and the Atlantic Ocean through Rockaway Inlet, a tidal channel behind the barrier spit of Rockaway Peninsula (Figure 1). The inlet channel is dredged for navigation and ranges in depth from 7 to 15 m. Tides are mainly semi-diurnal with a range of about 1.4 m.

The Jamaica Bay watershed is highly urbanized with more than 2.8 million residents (NYC DEP, 2018). The dominant freshwater input comes from four major municipal wastewater treatment plants with a total average discharge rate of about 10 m^3/s (Marsooli et al., 2018). During major rainfall events, watershed runoff, primarily via the storm sewer system, can substantially increase the freshwater input over periods of hours to days (Kasaei et al., 2025; Marsooli et al., 2018).

Jamaica Bay historically had extensive salt marsh area, but in recent decades substantial loss of marsh has occurred due to anthropogenic influences including dredging, shoreline hardening, and nutrient inputs (Peteet et al., 2018; Sanderson, 2016). Since the 1870s, total marsh area declined from 61 to 15 km^2 and intertidal unvegetated areas decreased from 17 to 4.6 km^2 (Orton et al., 2020). Without major watershed inputs, the primary source of sediment for Jamaica Bay is from the coastal zone. Observations and modeling estimated a mean landward sediment transport through the inlet of 55 ± 31 kt/y, with the dominant transport mechanism being asymmetry in the tidally induced bottom stress (Chant et al., 2021). Isotope-based studies of sediment deposition found a similar import of 74 ± 5 kt/y from marine sources based on ^{210}Pb, but a much larger and more uncertain estimate of 390 ± 140 kt/y using ^{234}Th (Renfro et al., 2016). Analyses of sediment cores indicate that the marsh

platform has been keeping up with recent sea-level rise with accretion rates up to 5 mm/y, albeit with reduced inorganic sediment compared with the older, deeper marsh soil, which is indicative of limited sediment supply (Peteet et al., 2018). Sea level rise at The Battery in New York Harbor has been about 3.4 mm/y in recent decades, but relative sea level rise in Jamaica Bay may be greater by about 1 mm/y due to groundwater extraction and soil compaction (Miller et al., 2013). Estimates of the sediment mass required for the current salt marsh area to maintain pace with sea level rise are greater than most of the estimates of sediment delivery (Chant et al., 2021). That study estimated that on average 115 kt/y of external sediment input is needed to maintain the current marsh area, or 1.5–2 times greater than most observational estimates.

The entrance to Jamaica Bay has repeatedly been identified (as far back as 1965) as a location where a storm surge barriers could reduce risk of coastal flooding (USACE, 2016), most recently as part of a regional Tentatively Selected Plan (US Army Corps of Engineers, New York District, 2022). The proposed surge barrier would be located at a constriction in Rockaway Inlet about 1 km in width and east of the Marine Parkway–Gil Hodges Bridge (Figure 1). The barrier would have both navigable gates (width ∼60 m and depth ∼8 m, floating sector gates) and auxiliary flow gates for tidal exchange (width ∼45 m, variable depth, vertical lift gates). All gates would close during storm surge events and otherwise remain open to tidal exchange. The total open flow opening in the conceptual design is about 57% of the existing flow cross-sectional area (US Army Corps of Engineers, New York District, 2022).

To evaluate the potential impacts of a barrier, we developed a nested-grid numerical ocean model using the Regional Ocean Modeling System (ROMS) with sediment transport through the COAWST framework. The circulation model is the ROMS, a three-dimensional, free-surface hydrodynamic model (Haidvogel et al., 2008; Shchepetkin & McWilliams, 2005). ROMS solves the three-dimensional Reynolds-averaged Navier-Stokes equations with hydrostatic and Boussinesq approximations using a finite difference approach on a horizontal curvilinear Arakawa C grid and vertically stretched terrain-following coordinates. Momentum and scalar transport equations for salinity, temperature, and suspended sediment include advection and vertical mixing with the Generalized Length Scale turbulence closure (Warner et al., 2005). The Community Sediment Transport Modeling System is integrated with ROMS through the Coupled Ocean-Atmosphere-Waves-Sediment Transport (COAWST) framework (Warner et al., 2008, 2010). Sediment transport can have multiple independent size classes, each with distinct attributes for grain size, settling velocity, and erodibility parameters. Erosion and deposition are based on flux formulations, and a bed model tracks the distribution of each size class.

The model developed for this study consists of three nested grids with increasing resolution focused on the barrier location (Figure 1). The outer Hudson model grid includes New York Harbor and the Hudson River estuary (Ralston, 2022). The Hudson model grid is 500 by 1200 grid cells, with typical along-estuary grid spacing of 100–150 m and across-estuary spacing of 20–60 m. Model boundaries are forced in New York Bight and western Long Island Sound with tidal harmonics plus non-tidal water level from NOAA observations at Sandy Hook, NJ (#8531680) and Kings Point, NY (#8516945). River discharge is input at the landward limit of the tidal Hudson based on USGS observations of the Mohawk at Cohoes (#1357500) and the Upper Hudson at Waterford (#1335754). Wind forcing is from the North American Mesoscale Forecast System (NAM) 12 km analysis product. Model bathymetry is based on data from New York State Department of Environmental Conservation, NOAA, and USACE (Ralston & Geyer, 2019). The model has 16 sigma layers that are evenly distributed in the vertical. The Hudson grid was calibrated with a bottom roughness (z_0) of 0.5 mm based on comparison with water level and salinity observations along the estuary (Ralston, 2022).

A nested grid approach is used to represent Jamaica Bay and the area around the proposed storm surge barrier. The Jamaica Bay grid is 500 by 700 grid cells, with east-west grid spacing of 30–50 m and north-south spacing of 25–40 m (Figure 1). The Jamaica Bay grid is a 5-to-1 refinement of a segment of the Hudson grid. Freshwater inputs to Jamaica Bay from four major wastewater treatment plants are point sources with a total discharge of 10 m^3/s. Boundary conditions for water level, velocity, salinity, and suspended sediment for the Jamaica Bay grid are extracted from the Hudson grid results. Bathymetry data is from high-resolution multibeam surveys in Jamaica Bay (Flood, 2011) along with the NOAA Continuously Updated Digital Elevation Model (Kasaei et al., 2025). The nested grids also have 16 sigma layers in the vertical, have the same z_0 of 0.5 mm, and use the same bathymetry data.

The second nested grid is a 5-to-1 refinement focused on the surge barrier location and uses two-way coupling with the Jamaica Bay grid. The Rockaway Inlet grid has 332 by 272 cells and horizontal resolution of about 6 m along the inlet and 5 m across the inlet. The geometry of the surge barrier was based on conceptual designs (US

Army Corps of Engineers, New York District, 2022). The barrier has two navigable openings that are each 61 m (200 ft) wide and 15 auxiliary openings for tidal exchange that are 46 m (150 ft) wide each. The total cross sectional area open to flow is 57% of that without the surge barrier in the proposed design. In the model grid, cells representing the fixed infrastructure for the gates are masked and the openings are scaled to the proposed design. The open flow area in the model with the barrier is 62% of the base case without the barrier. In the cases without a barrier, the Rockaway Inlet grid bathymetry is unaltered from present conditions.

Model setup for sediment transport follows previous studies of the region (Chant et al., 2021; Ralston, 2023; Ralston et al., 2013; Ralston & Geyer, 2017). Sediment is represented in four size classes: medium sand (settling velocity $w_s = 40$ mm/s, critical shear stress $\tau_b = 0.5$ N/m^2), fine sand ($w_s = 5$ mm/s, $\tau_b = 0.1$ N/m^2), medium silt ($w_s = 0.6$ mm/s, $\tau_b = 0.05$ N/m^2), and fine silt ($w_s = 0.1$ mm/s, $\tau_b = 0.05$ N/m^2). The initial bed sediment distributions for the Jamaica Bay and Rockaway Inlet grids were extracted from model results using the outer model grid. The nested model system was run for 2 months of tidal forcing to allow the initial bed distribution to adjust. The bed sediment distributions were reinitialized with the results from the spin-up period and given a uniform thickness of 0.1 m. Similarly, the bed sediment distributions were reinitialized after a 2-month spin-up with the barrier to reduce the influence of local erosion associated with the flow through the openings on the net sediment transport.

Two simulations were run, one with the baseline bathymetry and one with the Rockaway Inlet grid modified to represent the fixed infrastructure of the surge barrier. The geometry of the surge barrier is based on conceptual designs with two navigable openings (each 61 m wide) and 15 auxiliary openings (each 46 m wide) (US Army Corps of Engineers, New York District, 2022). In the grid with the barrier structure, the open flow area is 62% of the base case.

Simulations focused on a period of typical neap-spring variation, with the goal of capturing changes during non-extreme (open barrier) conditions. Leveraging prior model development (Kasaei et al., 2025), simulations were run with realistic offshore water level forcing and mean freshwater inputs over a period of about 45 days, and thus several spring-neap cycles. The simulation used water level forcing from September 2021 around the time of Tropical Storm Ida. The storm surge from Ida in the region was small, with a maximum excess non-tidal water level of 0.7 m, so storm surge gates would have remained open. Typically, barrier closure thresholds target water levels corresponding to 2-year to 5-year surge events (Orton et al., 2023), whereas the non-tidal water levels from Ida typically occur multiple times per year.

Model results were compared with water level measurements within the Jamaica Bay grid from USGS monitoring stations at Rockaway Inlet (#1311875) and Inwood (#1311850) and from a monitoring station at Bergen Basin operated by Stevens Institute of Technology (#SPJFKAP1) (Figure 1). The model reliably reproduced observed water level variability as measured by Nash–Sutcliffe efficiency (0.96, 0.95, 0.92 for Rockaway Inlet, Inwood, and Bergen Basin) or coefficient of determination ($r^2 = 0.98, 0.96, 0.93$). Other simulation periods that were evaluated for barrier impacts on flow and transport showed similar results. The dates of the model period are not important, so results are shown in terms of time since the start of the simulation.

3. Results

3.1. Alterations to Flow and Stratification

The reduction in cross-sectional area with the barrier infrastructure causes acceleration of the tidal flow and increased velocities downstream of the openings (Figure 2). Depth-averaged velocities in the openings reach 1.5 m/s during maximum flood tide and 1.3 m/s during ebbs, compared with maximum velocities without the barrier of 0.8–0.9 m/s (Figure 3). The lateral distribution of flow in the inlet is also altered. Without the barrier, the strongest tidal velocities occur in the deeper center of the channel. With the barrier, the flow spreads more uniformly across the inlet such that velocity increase is greater on the sides than in the center (Figure 3). Downstream of the barrier, flow separation creates regions of low velocity and recirculation (Figure 2).

The acceleration through the openings is driven by a sharp water level difference across the barrier (Figure 2), causing increased bottom stress and form drag and a reduction in tidal energy (Ralston, 2022). The water level gradient in this example is about 0.05 m across less than 100 m. For comparison, typical water level slopes along the tidal Hudson are around 10^{-5}, so the equivalent water level decrease would occur over 5 km. The example

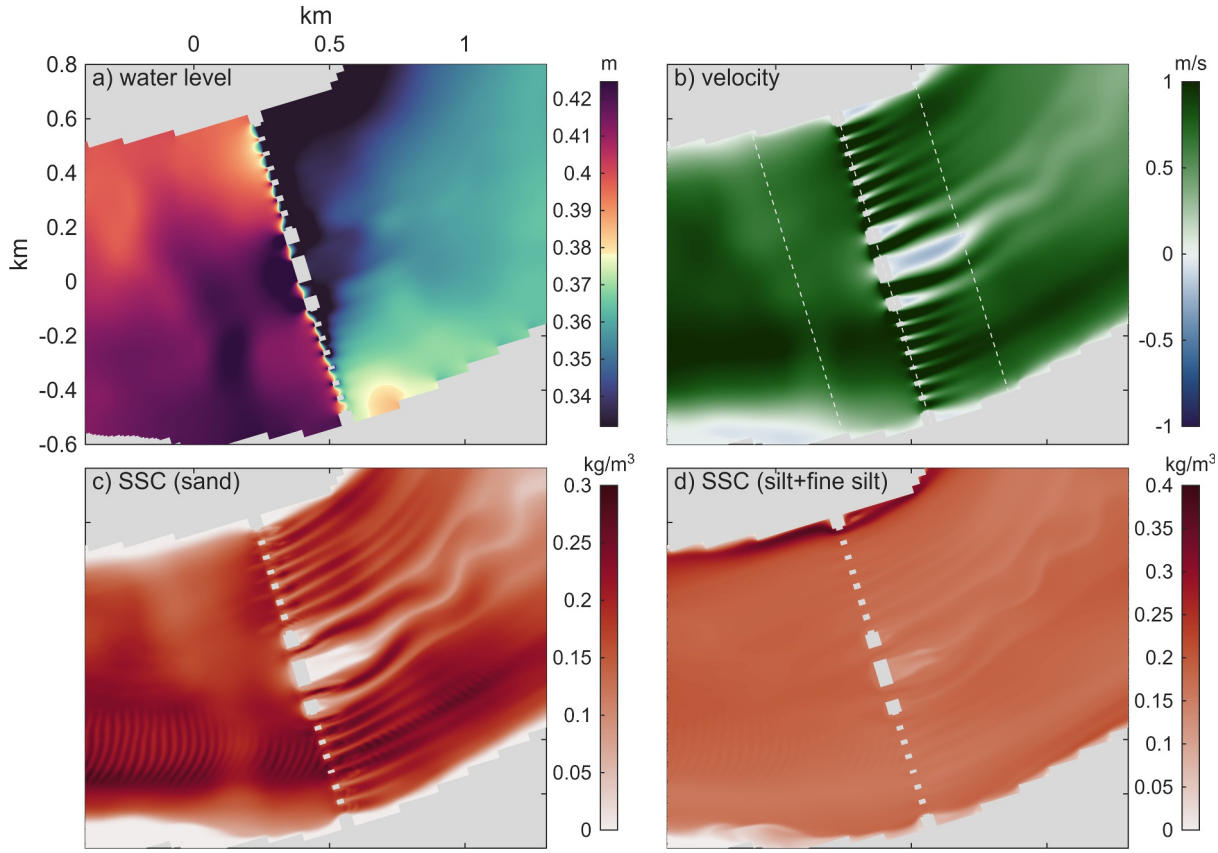

Figure 2. Instantaneous conditions around the barrier during a spring flood tide (10.92 d): (a) water level; (b) depth-averaged velocity; (c) near-bottom suspended sediment concentration (SSC) of fine sand; (d) SSC of medium silt and fine silt. Dashed lines in (b) mark velocity cross-sections in Figure 3.

shown is around maximum flood during spring tide conditions; for weaker forcing conditions the water level gradient through the barrier is less.

As a result of the increased drag, the tidal amplitudes inside Jamaica Bay (e.g., at Bergen Basin and Inwood, Figure 1) decrease by about 1.0% with the barrier compared to without. The decreases in tidal amplitude are less than the 5%–15% reductions found for some other surge barriers (Du et al., 2017; Nienhuis & Smaal, 1994; Ralston, 2022). The semidiurnal M_2 is the dominant tidal constituent with amplitudes of 0.72–0.82 m, and reductions in M_2 are similar to the total decrease of around 1%. The quarterdiurnal M_4 is smaller in magnitude, ranging from 0.044 m outside the bay to 0.059 m inside. However, the fractional reduction in M_4 due to the barrier is around 11%, much greater than for M_2.

Increased tidal velocities can cause an increase in turbulent mixing, potentially decreasing salinity stratification and weakening the estuarine exchange flow (Ralston, 2022). For Jamaica Bay, those effects are relatively small, which is consistent with previous analyses (Fischbach et al., 2018). The direct freshwater input of 10 m^3/s from wastewater treatment corresponds to a mean seaward velocity of about 0.005 m/s at the inlet. Correspondingly, the mean salinity inside the bay is relatively high at 27 psu and stratification is weak, typically less than 1 psu. The model results show small differences in stratification with the barrier. In the inlet and near the barrier, stratification is slightly reduced due to the increased velocities and greater mixing (Figure 4). The differences in mean stratification are greater during spring tides than during neaps, but the differences are small (<0.1 psu). Farther from the barrier, the stratification increases slightly during neap tides, which is consistent with the reduction in tidal amplitude. Overall, the changes in salinity and stratification are minor because of the modest freshwater inflows to the bay.

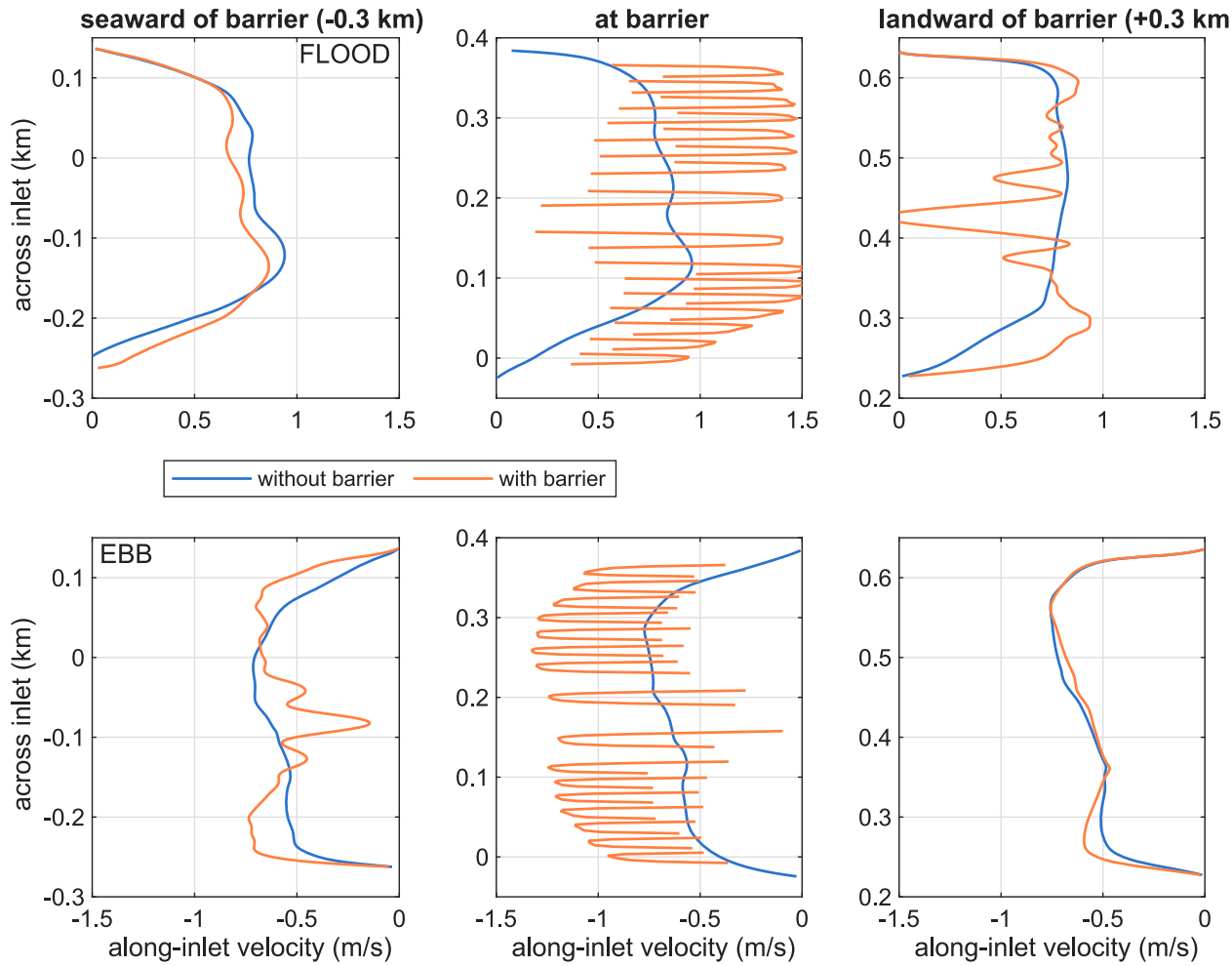

Figure 3. Comparison of depth-averaged velocity without and with the barrier during spring tides. (top panels) Flood tide (10.92 d, as in Figures 2 and 5) velocity across inlet seaward of barrier by 0.3 km (left), at the barrier (center), and landward by 0.3 km (right). (bottom panels) Ebb tide (11.17 d, as in Figure 5) velocity at the same cross-sections; cross-section locations are marked in Figure 2b.

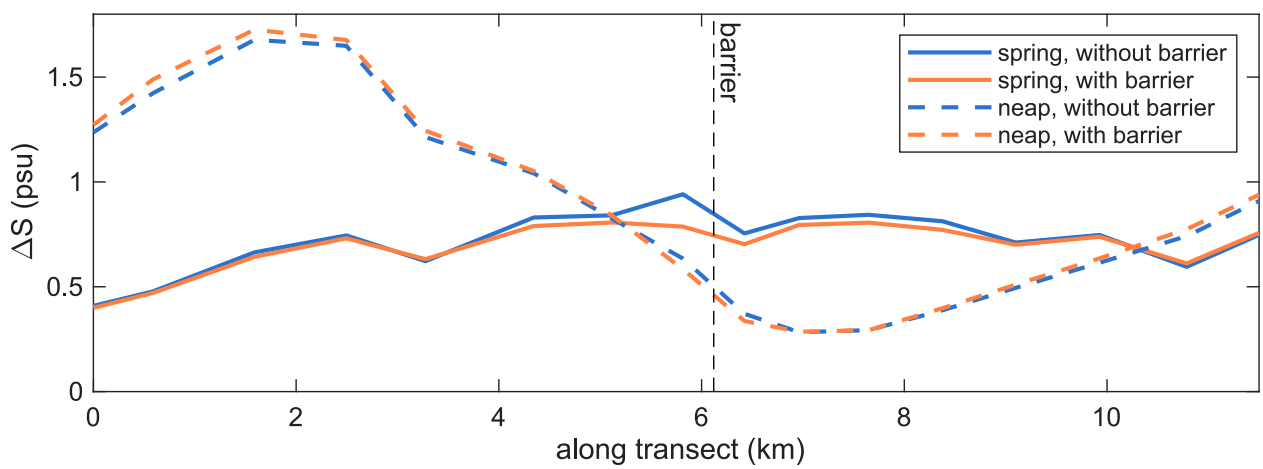

Figure 4. Stratification along a transect through Rockaway Inlet and along North Channel. Spring and neap tide averages are shown with and without the barrier. Transect location is marked in Figure 1.

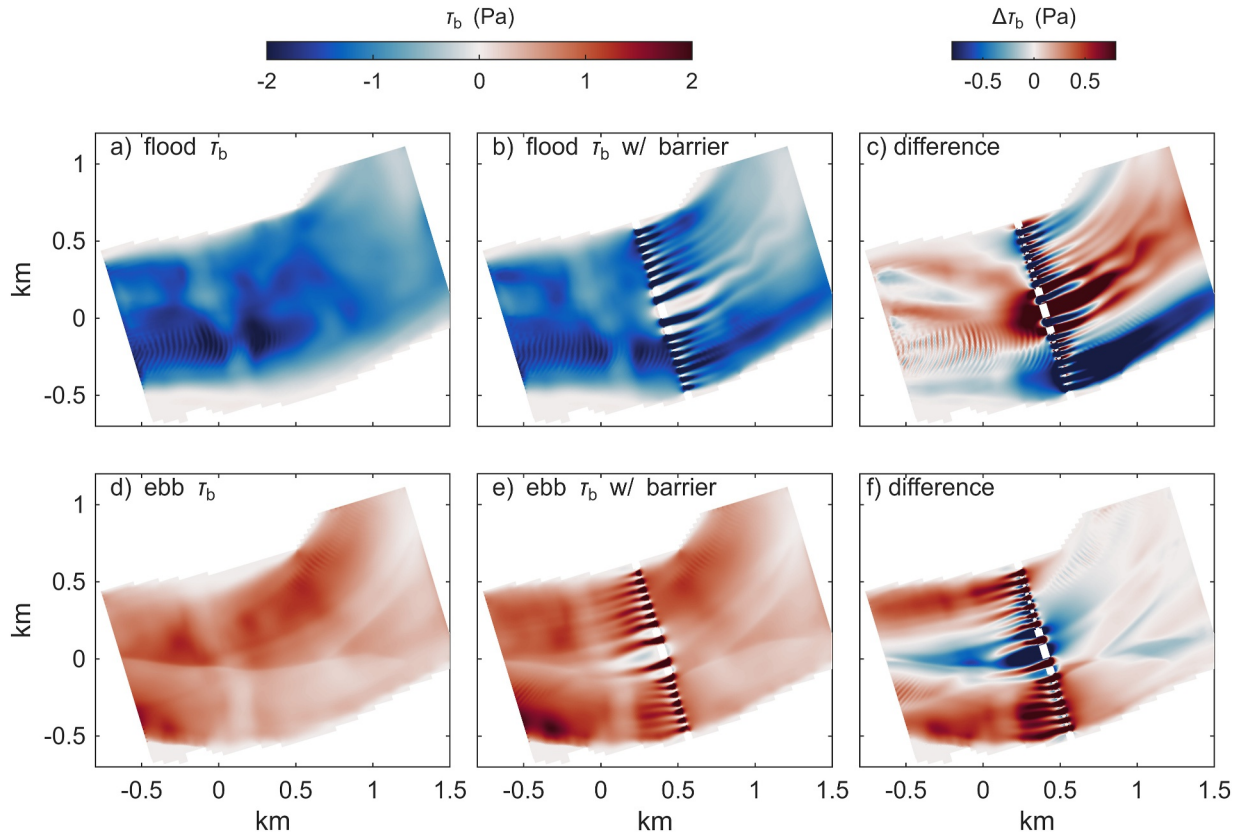

Figure 5. Example instantaneous bottom stress (τ_b) without and with the barrier. (a) flood tide without the barrier (10.92 d, as in Figures 2 and 3); (b) flood tide with the barrier; (c) difference between the flood cases, where negative values represent stronger flood-oriented flow; (e) ebb tide without the barrier (11.17 d, as in Figure 3); (d) ebb tide with the barrier; (f) difference between the ebb cases, where positive values represent stronger ebb-oriented flow.

3.2. Alterations to Bottom Stress

Increased tidal velocities through barrier openings correspond to increased bottom stress and bed sediment resuspension. Additionally, changes in tidal asymmetry can alter the net sediment transport over many tidal cycles. With the barrier, depth-averaged tidal velocities during bloth flood and ebb increase by approximately 50% due to the jets at the flow constriction (Figure 3), increasing bottom stress within about 0.5 km downstream of the openings. During flood tides the bottom stress becomes more negative (opposing the positive tidal velocity) and during ebbs the stress becomes more positive (Figure 5). These local increases in stress enhance sediment resuspension and bed erosion, which can require engineering measures to limit bed scour (Broekema et al., 2018). The lateral redistribution of flow also increases bottom stress on the lateral shoals. Both flood and ebb stresses intensify downstream of the barrier, while stresses in the main channel decrease (Figure 5).

The changes in bottom stress extend to larger spatial scales than the jets at the barrier openings (Figure 6). Mean stresses are altered within about 2 km of the barrier, primarily due to the lateral redistribution of flow. Farther from the barrier, the changes in stress are less than 0.1 Pa, a 10%–20% difference relative to the mean. Mean stresses during flood tides decrease in magnitude landward of the barrier, except for the southern part of the inlet. During ebbs, bottom stresses increase seaward of the barriers except in the central channel due to the flow redistribution.

Overall, the maximum bottom stresses are reduced by the barrier in the channel center and increased on the lateral shoals (Figure 6). Bottom stresses during spring tides exceed 1.5 Pa in the inlet, and differences with the barrier are 0.1–0.2 Pa. The decreases in stress relative to the baseline are fractionally greater landward of the barrier (~20%–30%) than seaward (~5%–10%).

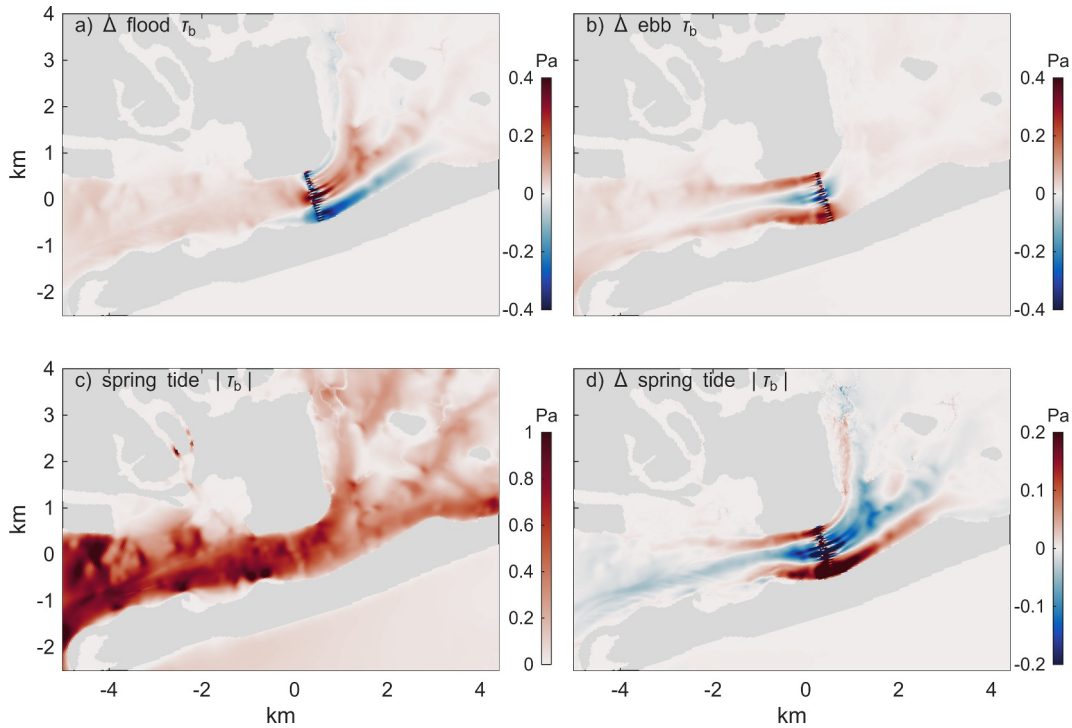

Figure 6. Changes in bottom stress (τ_b), plotting the barrier case minus the baseline. (a) Difference in mean flood-tide τ_b, where negative values represent stronger flood-oriented flows with the barrier. (b) Difference in mean ebb-tide τ_b, where positive values represent stronger ebb-oriented flows with the barrier. (c) Mean bottom stress amplitude during spring tides without the barrier. (d) Difference in mean bottom stress amplitude with the barrier.

3.3. Alterations to Sediment Transport

The influence of the barrier on sediment transport appears in the integrated transport by sediment size class (Figure 7). Sediment transport in the inlet is landward for all the size classes both with and without the barrier. The sediment import, or increasing cumulative transport, occurs primarily during spring tides, whereas net transport during neap tides is negligible. About 50% of the net landward transport occurs during spring tides, defined here as the largest 25% of tidal ranges. Correspondingly, neap tides (smallest 25%) account for just a few percent of the net transport. The overall rate of sediment transport in the model is greater than most previous estimates from observations and modeling (Chant et al., 2021; Renfro et al., 2016), which likely is due to uncertainty in the initial conditions for bed sediment composition. An estimate based on ^{210}Pb deposition in muddy subtidal sediments found fine sediment import was 74 ± 5 kt/y, and scaling the deposition up to all of the subtidal area of the bay would correspond to ∼190 kt/y (Renfro et al., 2016). The same study estimated sediment import based on ^{234}Th deposition rates at 390 ± 140 kt/y. Water column sediment flux measurements in Rockaway Inlet estimated 55 ± 31 kt/y (Chant et al., 2021), and previous modeling studies of different periods found annualized import rates of 24–74 kt/y (Chant et al., 2021; Donatelli et al., 2020). For the purposes of this study, the specific value of the sediment import rate is less important than the relative changes with the barrier.

Differences in the cumulative sediment transport with the barrier are greatest for the fine sand size class (Figure 7). Over the simulation period, the total transport of fine sand (5 mm/s) into the bay is reduced by about 20% with the barrier. Landward transport of medium silt (0.6 mm/s) decreases by about 3%, and transport of fine silt (0.1 mm/s) is essentially unchanged with or without the barrier.

To diagnose the influence of the barrier on sediment transport capacity we consider the velocity cubed along the inlet (Figure 8). As an approximation, suspended sediment concentration (SSC) increases with velocity (U) squared through the influence on bottom stress and resuspension, so tidal transport that goes as $U \times$ SSC has a cubic velocity dependency (Bagnold, 1966; Groen, 1967). The barrier influences both the tidal velocity amplitude

10.1029/2025EF007875

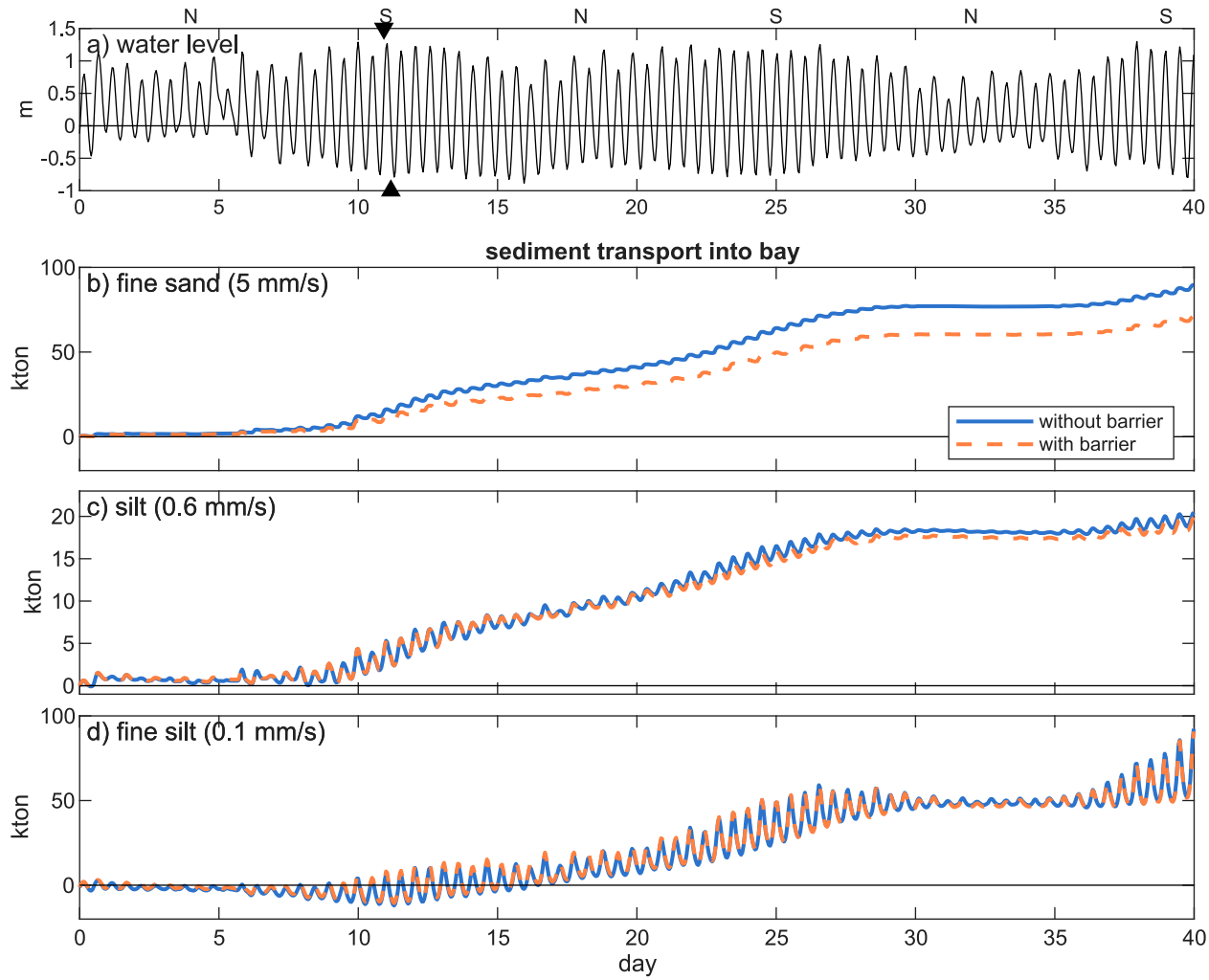

Figure 7. Cumulative sediment transport into Jamaica Bay without and with the barrier. (a) water level; (b) fine sand; (c) medium silt; (d) fine silt. "S" and "N" along top panel indicate spring and neap tides. Triangular markers in (a) show timing of flood and ebb tides illustrated in Figures 2, 3, and 5.

and the asymmetry between flood and ebb. We focus here on spring tides because they disproportionately account for the net transport, and laterally average U^3 across the inlet.

Overall, the barrier slightly reduces the average U^3 along the inlet, which is consistent with the decrease in tidal amplitude and reduction in landward sediment transport (Figure 8a). During flood tides, the reduction in U^3 is less notable landward of the barrier because velocity jets through the openings help offset the overall decrease in tidal amplitude. Similarly, during ebb tides the jets seaward of the barrier openings locally increase U^3 and mask the reductions in tidal amplitude compared to the baseline case. The magnitude of U^3 is greater during flood tide than during ebb, consistent with the net landward sediment transport.

As suggested by the changes in U^3, transport of fine sand decreases with the barrier (Figure 8b). This is primarily due to decreased landward transport during the flood tide both landward and seaward of the barrier. During ebbs, fine sand transport is essentially unchanged landward of the barrier but becomes slightly more seaward outside the barrier. The tidal jets through the barrier openings favor landward sediment transport during floods and seaward transport during ebbs, leading to a net divergence in sediment transport capacity.

In this inlet and other lagoonal systems, the landward sediment transport is mainly due to flood-dominant velocities from overtides (Friedrichs & Aubrey, 1988; Speer & Aubrey, 1985). The U^3 dependence of sediment transport capacity amplifies any flood-ebb asymmetries in the tidal velocity, and the minimal freshwater input reduces the influence of estuarine circulation on sediment transport (Burchard et al., 2018). We quantify the tidal

10.1029/2025EF007875

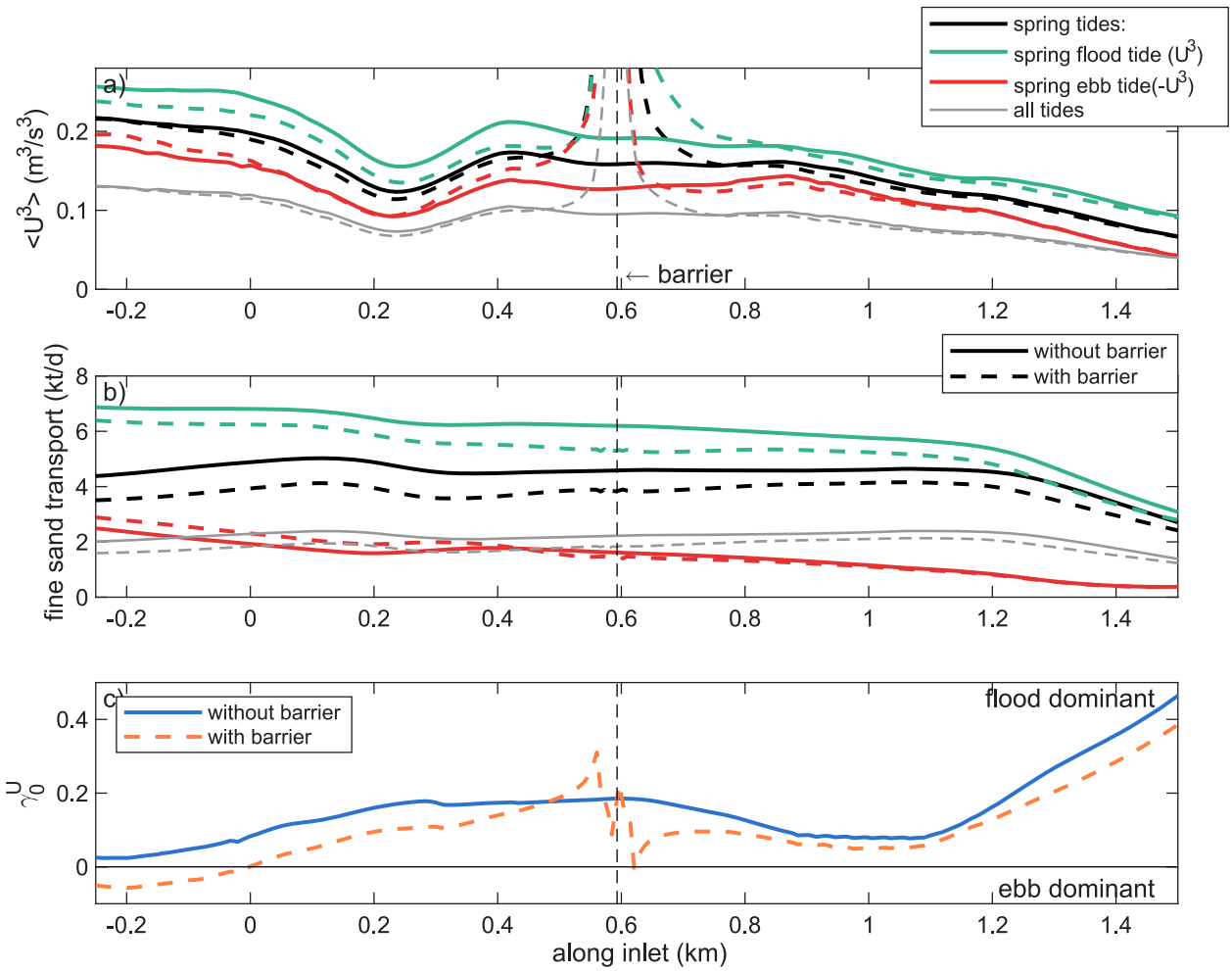

Figure 8. Sediment transport capacity along the inlet without and with the barrier. (a) Cross-section averaged, depth-averaged velocity cubed ($<U^3>$) versus distance along the inlet, averaged for spring tides (black lines), spring tide floods (green lines), spring tide ebbs (red lines), and all tidal conditions (gray lines), without the barrier as solid lines and with the barrier as dashed lines. The sign is reversed for ebb $<U^3>$ to facilitate comparison with the others. Barrier location is marked with a vertical dashed line. (b) Fine sand transport versus distance along the inlet. (c) Velocity skewness ($\gamma_0{}^U$) without (solid line) and with the barrier (dashed line), where positive values are flood-dominant.

asymmetry in the inlet with the velocity skewness ($\gamma_0{}^U$), or the normalized third moment about the mean (Nidzieko & Ralston, 2012). Positive values for $\gamma_0{}^U$ indicate velocity asymmetry favorable for landward transport, and vice versa. With the barrier, velocity skewness generally decreases by 20%–50% compared to $\gamma_0{}^U$ without the barrier, consistent with the decrease in tidal amplitude (Figure 8c). The decreases in $\gamma_0{}^U$ are greater on the seaward side of the barrier, and $\gamma_0{}^U$ can even change sign to become ebb-dominant, due to the enhanced ebb velocities through barrier openings.

The differences in tidal currents and sediment transport with the barrier lead to differences in bed sediment erosion and deposition (Figure 9). Near the barrier, increased velocities and bed stress due to the lateral redistribution of flow increases erosion on the shoals, particularly on the south side of the inlet. Correspondingly, reduced velocities in the channel increase sediment deposition with the barrier. Inside the bay, the barrier case has less bed sediment than the baseline, particularly in the main channel connecting to the northern parts of the bay. Sediment accumulation increases with the barrier downstream from the increased velocities on the south side of the inlet. Consistent with the sediment flux calculations, the total sediment mass in the bay is less with the barrier than without, primarily due to the differences in import of fine sand.

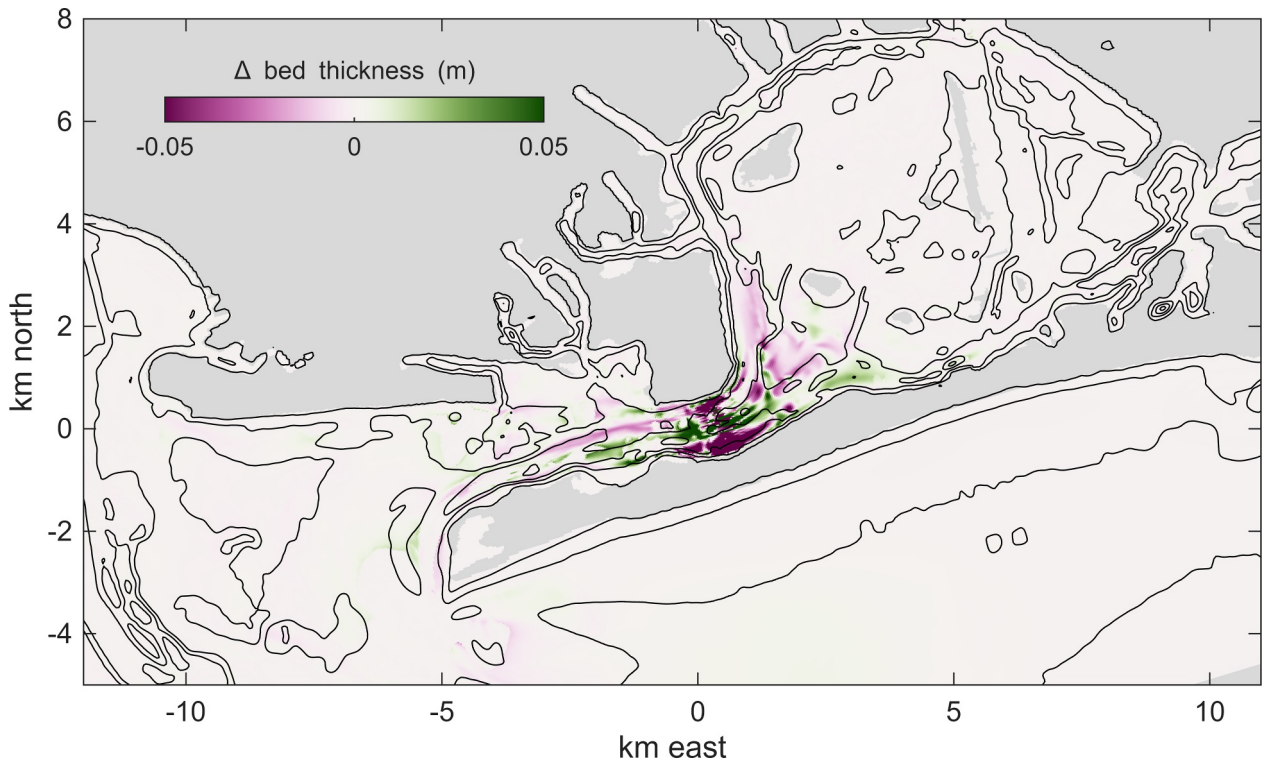

Figure 9. Differences in bed sediment thickness with the barrier over the simulation.

4. Discussion and Conclusion

For a lagoonal estuary like Jamaica Bay, the impacts of a surge barrier on sediment transport result from a decrease in tidal energy and the velocity asymmetry from flow through the barrier openings. In lagoonal estuaries, sediment is primarily delivered from offshore due to tidal velocity asymmetry. Nonlinear tidal dynamics amplify M_4 to create flood tide currents that are shorter duration and faster than ebbs (Friedrichs & Aubrey, 1988; Speer & Aubrey, 1985). Sediment transport scales approximately with velocity cubed, so flood-dominant velocities result in net landward sediment transport (Dronkers, 1986; Van de Kreeke & Robaczewska, 1993). The increased drag with the barrier reduces the tidal energy and therefore the landward sediment transport. While the overall reduction in tidal amplitude is a modest 1%, the fractional decrease in M_4 that is 10 times larger leads to the 20% reduction in import of fine sand to the bay. The M_4 overtide results from the variation in wave speed with tidal water level and depends on (a/h), or the ratio of the tidal water level amplitude (a) to the mean water depth (h) (Friedrichs & Aubrey, 1988). Thus, the generation of flood dominant currents and associated landward sediment transport is common to shallow tidal flows and we expect similar impacts from barrier infrastructure in other lagoonal systems with restricted inlets. Note that this study did not examine how transport and retention of watershed sediment input from precipitation events might be altered by barrier dynamics, which may be particularly relevant to finer sediment.

The alterations to sediment transport are more substantial for fine sand than for medium and fine silt (Figure 6). Similarly, for the Eastern Scheldt barrier the decrease in sediment flux was greater for sand than for finer sediment (de Vet et al., 2024). While sediment transport generally has a cubic-dependence on tidal velocity, the scaling depends on sediment characteristics (Bagnold, 1966; Groen, 1967). Finer sediment has a lower threshold for resuspension and is more uniformly distributed in the water column so is less sensitive to the decreases in tidal velocity than sand. The barrier substantially influences velocity and stress over spatial scales of 2–3 km (Figure 6), similar to the frictional length scale for a jet of H/C_d where H is the water depth (10 m) and C_d is the drag coefficient (3×10^{-3}) (Hench & Luettich, 2003). The advective time scale for tidal currents (~1 m/s) over this jet distance is about 1 hr. The settling time scale for fine sand ($H/w_s = 0.5$ hr) is shorter than this advective

time, whereas settling times for silt (5 hr) and fine silt (28 hr) are substantially longer and thus less likely to be affected by the velocity perturbations at the barrier.

The changes in sediment flux through the barrier can induce morphological changes inside the estuary. For example, in the Eastern Scheldt reductions in tidal amplitude shifted tidal channels out of equilibrium and caused erosion of tidal flats (de Vet et al., 2024; Eelkema et al., 2013). The Eastern Scheldt barrier also altered morphological activity on the ebb-tide delta due to decreased tidal currents and sediment supply (Eelkema et al., 2013). Alterations in sediment transport associated with the Venice Lagoon barrier were projected to increase wave-driven erosion of tidal flats, reduce delivery of sediment to marshes, and promote infilling of tidal channels (Tognin et al., 2022). Correspondingly, barrier operations during storm events can potentially be optimized to reduce impacts on estuarine morphology and marsh habitat while still meeting surge protection objectives (Michielotto et al., 2025).

For Jamaica Bay, the tidal amplitude decreases are small and any changes in channel morphology would likely be limited to a few km of the barrier (Figures 6 and 9). The interior of Jamaica Bay has marsh area that is threatened by insufficient supply of fine sediment (Chant et al., 2021; Peteet et al., 2018), but the results here indicate that fine sediment transport through the open barrier would not be substantially altered. However, reductions in sand supply may accelerate the loss of shallow subtidal and intertidal areas, potentially increasing wave energy exposure at marsh edges. Loss of shallow subtidal and intertidal areas along with deepening of channels for navigation over the past 150 years has been linked to amplification of storm surge within the bay (Orton et al., 2020). More generally, sediment supply is well established as a primary factor controlling marsh resilience to sea level rise, both globally (Kirwan et al., 2010; Ladd et al., 2019; Schile et al., 2014) and regionally along the US East Coast (Baranes et al., 2022; Ganju et al., 2015; Teng et al., 2025). Decreases in sediment import from the coastal zone due to flow alterations by surge barriers could therefore affect long-term survival of marshes in similar lagoonal systems.

A consideration not examined here is how sediment supply to marshes during storm events would be affected by barrier closures. Studies of the Venice Lagoon found that marsh accretion was reduced by a surge barrier due to less frequent marsh inundation and more sediment accumulation in the channels (Tognin et al., 2022). For Jamaica Bay, suspended sediment concentrations outside the mouth increased with wave-driven resuspension during a storm event, thereby approximately doubling sediment import into the bay compared to conditions without waves (Chant et al., 2021). Similarly, simulations of sediment transport during Hurricane Sandy found an import of about 9 kt of sand and mud (Hu et al., 2018), or more than 10% of the annual average sediment supply in just a few days. Storm surge water levels increase inundation of the marsh and other low elevation regions, making storm events disproportionately important for the total sediment delivery to the marsh (Castagno et al., 2018). Thus, alterations to sediment transport by barrier closures are also likely to have negative impacts on marsh sustainability.

Effects of surge barriers on sediment transport differ strongly between estuary types. For example, the estuarine dynamics of Jamaica Bay are substantially different from the nearby partially mixed Hudson River. For both systems, barrier infrastructure would cause local acceleration of the flow, increased drag, locally increased turbulence and mixing, and decreased tidal amplitude (Ralston, 2022). These alterations would reduce the sediment transport through barriers, albeit for different reasons and with different consequences. A partially mixed estuary will have increased estuarine circulation and retain more of the fluvial sediment, exporting less offshore (Ralston, 2023). A lagoonal estuary will have reduced landward sediment transport from offshore due to the changes in tidal amplitude and velocity asymmetry. The comparison between systems demonstrates that estuarine dynamics influence potential barrier impacts, with the shallow bathymetry, modest watershed inputs, and predominance of tidal exchange making lagoonal estuaries particularly vulnerable to reductions in sediment supply.

Conflict of Interest

The authors declare no conflicts of interest relevant to this study.

Availability Statement

The data that support the findings of this study are available at https://doi.org/10.5281/zenodo.18967501 (Ralston, 2026). *Software Availability*: The source code for the Coupled Ocean, Atmosphere, Waves, and Sediment Transport (COAWST) model is available at https://github.com/DOI-USGS/COAWST (Warner, 2026). The code is in the public domain. Details on the COAWST model are described in (Warner et al., 2010). Model input files for the simulations presented here are available at https://doi.org/10.5281/zenodo.18967501 (Ralston, 2026).

Acknowledgments
This research has been supported by the US Geological Survey through the Extending Government Funding and Delivering Emergency Assistance Act (Public Law 117-43) with award no. G22AC00398 under the North Atlantic Coast Co-operative Ecosystems Study Unit.

References

Bagnold, R. A. (1966). *An approach to the sediment transport problem from general physics*. US Government Printing Office.

Bakker, C., Herman, P. M. J., & Vink, M. (1990). Changes in seasonal succession of phytoplankton induced by the storm-surge barrier in the Oosterschelde (SW Netherlands). *Journal of Plankton Research*, *12*(5), 947–972. https://doi.org/10.1093/plankt/12.5.947

Baranes, H. E., Woodruff, J. D., Geyer, W. R., Yellen, B. C., Richardson, J. B., & Griswold, F. (2022). Sources, mechanisms, and timescales of sediment delivery to a new England salt Marsh. *Journal of Geophysical Research: Earth Surface*, *127*(3), e2021JF006478. https://doi.org/10.1029/2021JF006478

Brand, A. D., Kothuis, B., & Prooijen, B. (2016). The Eastern scheldt survey. *A Concise Overview of the Estuary Pre- and Post Barrier. Part 2: SURVEY*. https://doi.org/10.13140/RG.2.1.1455.5764

Broekema, Y. B., Labeur, R. J., & Uijttewaal, W. S. J. (2018). Observations and analysis of the horizontal structure of a tidal jet at deep scour holes. *Journal of Geophysical Research: Earth Surface*, *123*(12), 3162–3189. https://doi.org/10.1029/2018JF004754

Burchard, H., Schuttelaars, H. M., & Ralston, D. K. (2018). Sediment trapping in estuaries. *Annual Review of Marine Science*, *10*(1), 371–395. https://doi.org/10.1146/annurev-marine-010816-060535

Castagno, K. A., Jiménez-Robles, A. M., Donnelly, J. P., Wiberg, P. L., Fenster, M. S., & Fagherazzi, S. (2018). Intense storms increase the stability of tidal bays. *Geophysical Research Letters*, *45*(11), 5491–5500. https://doi.org/10.1029/2018gl078208

Chant, R. J., Ralston, D. K., Ganju, N. K., Pianca, C., Simonson, A. E., & Cartwright, R. A. (2021). Sediment budget estimates for a highly impacted embayment with extensive wetland loss. *Estuaries and Coasts*, *44*(3), 608–626. https://doi.org/10.1007/s12237-020-00784-3

Chen, Z., Orton, P., & Wahl, T. (2020). Storm surge barrier protection in an era of accelerating sea-level rise: Quantifying closure frequency, duration and trapped River flooding. *Journal of Marine Science and Engineering*, *8*(9), 725. https://doi.org/10.3390/jmse8090725

Chen, Z., & Orton, P. M. (2023). Effects of storm surge barrier closures on Estuary saltwater intrusion and stratification. *Water Resources Research*, *59*(3), e2022WR032317. https://doi.org/10.1029/2022WR032317

de Vet, P. L. M., van Prooijen, B. C., Herman, P. M. J., Bouma, T. J., van Maren, D. S., Walles, B., et al. (2024). Response of estuarine morphology to storm surge barriers, closure dams and sea level rise. *Geomorphology*, *467*, 109462. https://doi.org/10.1016/j.geomorph.2024.109462

Donatelli, C., Kalra, T. S., Fagherazzi, S., Zhang, X., & Leonardi, N. (2020). Dynamics of marsh-derived sediments in lagoon-type estuaries. *Journal of Geophysical Research: Earth Surface*, *125*(12), e2020JF005751. https://doi.org/10.1029/2020JF005751

Dronkers, J. (1986). Tide-induced residual transport of fine sediment. In J. Van De Kreeke (Ed.), *Lecture notes on coastal and estuarine studies* (Vol. 16, pp. 228–244). American Geophysical Union. https://doi.org/10.1029/LN016p0228

Du, J., Shen, J., Bilkovic, D. M., Hershner, C. H., & Sisson, M. (2017). A numerical modeling approach to predict the effect of a storm surge barrier on hydrodynamics and long-term transport processes in a partially mixed estuary. *Estuaries and Coasts*, *40*(2), 387–403. https://doi.org/10.1007/s12237-016-0175-0

Eelkema, M., Wang, Z. B., Hibma, A., & Stive, M. J. F. (2013). Morphological effects of the Eastern scheldt storm surge barrier on the ebb-tidal Delta. *Coastal Engineering Journal*, *55*(3), 1350010-1–1350010-26. https://doi.org/10.1142/S0578563413500101

Finotello, A., Tognin, D., Carniello, L., Ghinassi, M., Bertuzzo, E., & D'Alpaos, A. (2023). Hydrodynamic feedbacks of Salt-Marsh loss in the shallow microtidal back-barrier lagoon of Venice (Italy). *Water Resources Research*, *59*(3), e2022WR032881. https://doi.org/10.1029/2022WR032881

Fischbach, J. R., Knopman, D., Smith, H., Orton, P. M., Sanderson, E. W., Fisher, K., et al. (2018). *Building resilience in an urban coastal environment: Integrated, Science-Based Planning in Jamaica Bay*. RAND Corporation. Retrieved from https://www.rand.org/content/dam/rand/pubs/research_reports/RR2100/RR2193/RAND_RR2193.pdf

Flood, R. (2011). *High-Resolution bathymetric and backscatter mapping in Jamaica Bay (Final Report to the National Park Service)*. State University of New York at Stony Brook.

Friedrichs, C. T., & Aubrey, D. G. (1988). Non-linear tidal distortion in shallow well-mixed estuaries: A synthesis. *Estuarine, Coastal and Shelf Science*, *27*(5), 521–545. https://doi.org/10.1016/0272-7714(88)90082-0

Ganju, N. K., Kirwan, M. L., Dickhudt, P. J., Guntenspergen, G. R., Cahoon, D. R., & Kroeger, K. D. (2015). Sediment transport-based metrics of wetland stability. *Geophysical Research Letters*, *42*(19), 7992–8000. https://doi.org/10.1002/2015GL065980

Groen, P. (1967). On the residual transport of suspended matter by an alternating tidal current. *Netherlands Journal of Sea Research*, *3*(4), 564–574. https://doi.org/10.1016/0077-7579(67)90004-X

Haidvogel, D. B., Arango, H., Budgell, W. P., Cornuelle, B. D., Curchitser, E., Di Lorenzo, E., et al. (2008). Ocean forecasting in terrain-following coordinates: Formulation and skill assessment of the Regional Ocean Modeling System. *Journal of Computational Physics*, *227*(7), 3595–3624. https://doi.org/10.1016/j.jcp.2007.06.016

Hench, J. L., & Luettich, R. A. (2003). Transient tidal circulation and momentum balances at a shallow inlet. *Journal of Physical Oceanography*, *33*(4), 913–932. https://doi.org/10.1175/1520-0485(2003)33<913:ttcamb>2.0.co;2

Hu, K., Chen, Q., Wang, H., Hartig, E. K., & Orton, P. M. (2018). Numerical modeling of salt marsh morphological change induced by Hurricane Sandy. *Coastal Engineering*, *132*, 63–81. https://doi.org/10.1016/j.coastaleng.2017.11.001

Kasaei, S., Orton, P. M., Ralston, D. K., & Warner, J. C. (2025). Pluvial and potential compound flooding in a coupled coastal modeling framework: New York City during post-tropical Cyclone Ida (2021). *Hydrology and Earth System Sciences*, *29*(8), 2043–2058. https://doi.org/10.5194/hess-29-2043-2025

Kirwan, M. L., Guntenspergen, G. R., D'Alpaos, A., Morris, J. T., Mudd, S. M., & Temmerman, S. (2010). Limits on the adaptability of coastal marshes to rising sea level. *Geophysical Research Letters*, *37*(23), L23401. https://doi.org/10.1029/2010GL045489

Kluijver, M., Dols, C., Jonkman, S. N., & Mooyaart, L. F. (2019). Advances in the planning and conceptual design of storm surge barriers – Application to the New York metropolitan area. *Coastal Structures*, *2019*, 326–336. https://doi.org/10.18451/978-3-939230-64-9_033

Ladd, C. J. T., Duggan-Edwards, M. F., Bouma, T. J., Pagès, J. F., & Skov, M. W. (2019). Sediment supply explains long-term and large-scale patterns in Salt Marsh lateral expansion and erosion. *Geophysical Research Letters*, *46*(20), 11178–11187. https://doi.org/10.1029/2019GL083315

Louters, T., Berg, J. H., & Mulder, J. P. M. (1998). Geomorphological changes of the oosterschelde tidal System during and after the implementation of the Delta Project. *Journal of Coastal Research*, *14*(3), 1134–1151.

Marsooli, R., Orton, P. M., Fitzpatrick, J., & Smith, H. (2018). Residence time of a highly urbanized estuary: Jamaica Bay, New York. *Journal of Marine Science and Engineering*, *6*(2), 44. https://doi.org/10.3390/jmse6020044

Matticchio, B., Carniello, L., Canesso, D., Ziggiotto, E., & Cordella, M. (2017). Recent changes in tidal propagation in the Venice Lagoon: Effects of changes in the inlet structure. *Commissione Di Studio Sui Problemi Di Venezia*, *3*, 157–183.

Michielotto, A., Finotello, A., Mel, R., Lazarus, E., Carniello, L., Tognin, D., & D'Alpaos, A. (2025). Reconciling flood-risk reduction and wetland resilience behind coastal floodgates. *Research Square*. https://doi.org/10.21203/rs.3.rs-7100485/v1

Miller, K. G., Kopp, R. E., Horton, B. P., Browning, J. V., & Kemp, A. C. (2013). A geological perspective on sea-level rise and its impacts along the U.S. mid-Atlantic coast. *Earth's Future*, *1*(1), 3–18. https://doi.org/10.1002/2013EF000135

Mooyaart, L. F., & Jonkman, S. N. (2017). Overview and design considerations of storm surge barriers. *Journal of Waterway, Port, Coastal, and Ocean Engineering*, *143*(4), 06017001. https://doi.org/10.1061/(ASCE)WW.1943-5460.0000383

Nidzieko, N. J., & Ralston, D. K. (2012). Tidal asymmetry and velocity skew over tidal flats and shallow channels within a macrotidal river delta. *Journal of Geophysical Research*, *117*(C3), 2011JC007384. https://doi.org/10.1029/2011JC007384

Nienhuis, P. H., & Smaal, A. C. (1994). The Oosterschelde estuary, a case-study of a changing ecosystem: An introduction. *The Oosterschelde Estuary (The Netherlands): A Case-Study of a Changing Ecosystem*, *1–14*, 1–14. https://doi.org/10.1007/978-94-011-1174-4_1

NYC DEP. (2018). Jamaica Bay watershed protection plan update 2018. Retrieved from https://www.nyc.gov/assets/dep/downloads/pdf/water/nyc-waterways/jamaica-bay/jamaica-bay-watershed-protection-plan-update-2018.pdf

Orton, P. M., Ralston, D., Van Prooijen, B., Secor, D., Ganju, N., Chen, Z., et al. (2023). Increased utilization of storm surge barriers: A research agenda on Estuary impacts. *Earth's Future*, *11*(3), e2022EF002991. https://doi.org/10.1029/2022EF002991

Orton, P. M., Sanderson, E. W., Talke, S. A., Giampieri, M., & MacManus, K. (2020). Storm tide amplification and habitat changes due to urbanization of a lagoonal estuary. *Natural Hazards and Earth System Sciences*, *20*(9), 2415–2432. https://doi.org/10.5194/nhess-20-2415-2020

Peteet, D. M., Nichols, J., Kenna, T., Chang, C., Browne, J., Reza, M., et al. (2018). Sediment starvation destroys New York City marshes' resistance to sea level rise. *Proceedings of the National Academy of Sciences*, *115*(41), 10281–10286. https://doi.org/10.1073/pnas.1715392115

Ralston, D. K. (2022). Impacts of storm surge barriers on drag, mixing, and exchange flow in a partially mixed estuary. *Journal of Geophysical Research: Oceans*, *127*(4), e2021JC018246. https://doi.org/10.1029/2021jc018246

Ralston, D. K. (2023). Changes in estuarine sediment dynamics with a storm surge barrier. *Estuaries and Coasts*, *46*(3), 678–696. https://doi.org/10.1007/s12237-023-01172-3

Ralston, D. K. (2026). Data for "Storm surge barriers reduce seaward sediment supply to lagoonal estuaries" [Dataset]. https://doi.org/10.5281/zenodo.18967501

Ralston, D. K., & Geyer, W. R. (2017). Sediment transport time scales and trapping efficiency in a tidal river. *Journal of Geophysical Research: Earth Surface*, *122*(11), 2042–2063. https://doi.org/10.1002/2017jf004337

Ralston, D. K., & Geyer, W. R. (2019). Response to channel deepening of the salinity intrusion, estuarine circulation, and stratification in an urbanized Estuary. *Journal of Geophysical Research: Oceans*, *124*(7), 4784–4802. https://doi.org/10.1029/2019JC015006

Ralston, D. K., Warner, J. C., Geyer, W. R., & Wall, G. R. (2013). Sediment transport due to extreme events: The Hudson River estuary after tropical storms Irene and Lee. *Geophysical Research Letters*, *40*(20). https://doi.org/10.1002/2013GL057906

Rasmussen, D. J., Buchanan, M. K., Kopp, R. E., & Oppenheimer, M. (2020). A flood damage allowance framework for coastal protection with deep uncertainty in Sea level rise. *Earth's Future*, *8*(3), e2019EF001340. https://doi.org/10.1029/2019EF001340

Renfro, A. A., Cochran, J. K., Hirschberg, D. J., Bokuniewicz, H. J., & Goodbred, S. L. (2016). The sediment budget of an urban coastal lagoon (Jamaica Bay, NY) determined using 234Th and 210Pb. *Estuarine, Coastal and Shelf Science*, *180*, 136–149. https://doi.org/10.1016/j.ecss.2016.06.008

Sanderson, E. W. (2016). Cartographic evidence for historical geomorphological change and wetland formation in Jamaica Bay, New York. *Northeastern Naturalist*, *23*(2), 277–304. https://doi.org/10.1656/045.023.0208

Scarpa, G. M., Davison, S., Manfè, G., Lorenzetti, G., Zaggia, L., & Braga, F. (2025). Suspended sediment dynamics at the inlets of Venice Lagoon: Unraveling the effects of storm surges and mobile barrier operations. *Journal of Hydrology*, *651*, 132588. https://doi.org/10.1016/j.jhydrol.2024.132588

Schile, L. M., Callaway, J. C., Morris, J. T., Stralberg, D., Parker, V. T., & Kelly, M. (2014). Modeling tidal marsh distribution with sea-level rise: Evaluating the role of vegetation, sediment, and Upland habitat in marsh resiliency. *PLoS One*, *9*(2), e88760. https://doi.org/10.1371/journal.pone.0088760

Shchepetkin, A. F., & McWilliams, J. C. (2005). The regional oceanic modeling system (ROMS): A split-explicit, free-surface, topography-following-coordinate oceanic model. *Ocean Modelling*, *9*(4), 347–404. https://doi.org/10.1016/j.ocemod.2004.08.002

Smaal, A. C., & Nienhuis, P. H. (1992). The eastern Scheldt (the Netherlands), from an estuary to a tidal bay: A review of responses at the ecosystem level. *Netherlands Journal of Sea Research*, *30*, 161–173. https://doi.org/10.1016/0077-7579(92)90055-J

Speer, P. E., & Aubrey, D. G. (1985). A study of non-linear tidal propagation in shallow inlet/estuarine systems Part II: Theory. *Estuarine, Coastal and Shelf Science*, *21*(2), 207–224. https://doi.org/10.1016/0272-7714(85)90097-6

Strauss, B. H., Orton, P. M., Bittermann, K., Buchanan, M. K., Gilford, D. M., Kopp, R. E., et al. (2021). Economic damages from Hurricane Sandy attributable to sea level rise caused by anthropogenic climate change. *Nature Communications*, *12*(1), 2720. https://doi.org/10.1038/s41467-021-22838-1

Temmerman, S., Meire, P., Bouma, T. J., Herman, P. M. J., Ysebaert, T., & De Vriend, H. J. (2013). Ecosystem-based coastal defence in the face of global change. *Nature*, *504*(7478), 79–83. https://doi.org/10.1038/nature12859

Teng, W., Yellen, B., Yu, Q., Ganju, N. K., Peck, E. K., Cook, T., & Woodruff, J. D. (2025). Marine-Sourced sediment supply supports Salt Marsh resilience to Sea level rise in the Northeastern US. *Geophysical Research Letters*, *52*(24), e2025GL118706. https://doi.org/10.1029/2025GL118706

Tognin, D., D'Alpaos, A., Marani, M., & Carniello, L. (2021). Marsh resilience to sea-level rise reduced by storm-surge barriers in the Venice Lagoon. *Nature Geoscience*, *14*(12), 906–911. https://doi.org/10.1038/s41561-021-00853-7

Tognin, D., Finotello, A., D'Alpaos, A., Viero, D. P., Pivato, M., Mel, R. A., et al. (2022). Loss of geomorphic diversity in shallow tidal embayments promoted by storm-surge barriers. *Science Advances*, *8*(13), eabm8446. https://doi.org/10.1126/sciadv.abm8446

US Army Corps of Engineers, Galveston District, & Texas General Land Office. (2021). Coastal Texas protection and ecosystem restoration feasibility Study -- final environmental impact statement

US Army Corps of Engineers, New York District. (2022). New York-New Jersey Harbor and tributaries coastal storm risk management feasibility Study (Draft integrated feasibility report and tier 1 environmental impact statement)

US Army Corps of Engineers, Philadelphia District. (2021). New Jersey back bays Coastal storm risk management draft integrated feasibility report and Tier1 environmental impact statement. Retrieved from https://www.nap.usace.army.mil/Portals/39/docs/Civil/NJBB/Draft-Report/NJ-Backbays-Main-Report-16Aug2021-Final-Revised.pdf

Van de Kreeke, J., & Robaczewska, K. (1993). Tide-induced residual transport of coarse sediment; application to the Ems estuary. *Netherlands Journal of Sea Research*, *31*(3), 209–220. https://doi.org/10.1016/0077-7579(93)90022-k

Warner, J. C. (2026). Coawst [Software]. *USGS*. Retrieved from https://github.com/DOI-USGS/COAWST

Warner, J. C., Armstrong, B., He, R., & Zambon, J. B. (2010). Development of a coupled ocean–atmosphere–wave–sediment transport (COAWST) modeling System. *Ocean Modelling*, *35*(3), 230–244. https://doi.org/10.1016/j.ocemod.2010.07.010

Warner, J. C., Sherwood, C. R., Arango, H. G., & Signell, R. P. (2005). Performance of four turbulence closure models implemented using a generic length scale method. *Ocean Modelling*, *8*(1), 81–113. https://doi.org/10.1016/j.ocemod.2003.12.003

Warner, J. C., Sherwood, C. R., Signell, R. P., Harris, C. K., & Arango, H. G. (2008). Development of a three-dimensional, regional, coupled wave, current, and sediment-transport model. *Computers & Geosciences*, *34*(10), 1284–1306. https://doi.org/10.1016/j.cageo.2008.02.012